Petroleum Science 23 (2026) 2698–2712

Contents lists available at ScienceDirect

Petroleum Science

journal homepage: www.keaipublishing.com/en/journals/petroleum-science

Original Paper

Effect of CO_2 pre-injection on fracture propagation morphology in shale reservoirs under CO_2 hybrid fracturing

Yu-Xi Zang [a,*], Feng-Xia Li [a], Hai-Zhu Wang [b], Zhi-Wen Huang [a], Tong Zhou [a], Jia Cui [a], Ning Li [a], Shou-Ceng Tian [b,c,**]

[a] State Key Laboratory of Shale Oil and Gas Enrichment Mechanisms and Efficient Development, Beijing, 100083, China
[b] State Key Laboratory of Petroleum Resources and Prospecting, China University of Petroleum (Beijing), Beijing, 102249, China
[c] College of Petroleum, China University of Petroleum-Beijing at Karamay, Karamay, 834000, Xinjiang, China

ARTICLE INFO

Article history:
Received 8 September 2025
Received in revised form
2 December 2025
Accepted 20 January 2026
Available online 23 January 2026

Edited by Meng-Jiao Zhou

Keywords:
CO_2 hybrid fracturing
Fracture propagation
Fracture morphology
Parameter optimization

ABSTRACT

Supercritical CO_2 fracturing, as a waterless fracturing technology, is attracting increasing attention in the shale oil reservoir development industry. In recent years, a novel CO_2 hybrid fracturing method has been proposed to integrate the advantages of both CO_2 fracturing and hydraulic fracturing. However, the specific effects of different pre-injection CO_2 conditions on the physical properties, mechanical characteristics, and crack propagation behavior of shale reservoirs remain unclear. This study utilized Chang-7 shale samples from the Ordos Basin and conducted CO_2 hybrid fracturing experiments under simulated high-temperature and high-pressure reservoir conditions, employing a self-developed experimental apparatus. Quantitative analysis of fracture propagation patterns under the influence of CO_2 pre-injection was performed based on CT scanning results. The findings reveal that: (1) Among different fracturing fluid systems, conventional hydraulic fracturing exhibits the highest breakdown pressure, pure CO_2 fracturing is intermediate, while CO_2 hybrid fracturing significantly reduces the breakdown pressure by 36.2% compared to hydraulic fracturing. (2) Employing CO_2 hybrid fracturing not only effectively increases fracture dimensions (length, width) but also substantially enhances fracture network complexity. (3) The CO_2 pre-injection soaking time significantly influences fracture morphology, with both fracture dimensions and structural complexity showing marked increases as soaking time extends. (4) Increasing formation pore pressure promotes the activation of bedding planes with relatively weaker mechanical strength, leading to significant enhancements in fracture length and complexity, but simultaneously restricts the widening of fracture apertures. The outcomes of this research provide a theoretical foundation for optimizing the design of operational parameters in CO_2 hybrid fracturing for shale oil reservoirs.

1. Introduction

Against the backdrop of global energy transition, unconventional hydrocarbon resources such as shale gas and tight oil have become strategic alternatives for energy security (Avanthi Isaka, et al., 2019; Zou et al., 2024). According to International Energy Agency (IEA) statistics, these resources constitute over 60% of the world's technically recoverable hydrocarbon reserves (Lopez et al., 2025). However, their economic exploitation faces fundamental challenges: reservoir permeabilities are typically below 0.1 mD, with pore-throat diameters predominantly at the nanoscale (10–200 nm) (Wang and Wang, 2022; Wang et al., 2020a; Yu et al., 2020). Conventional vertical well production cannot achieve commercial flow rates, necessitating large-scale volumetric fracturing (stimulated reservoir volume, SRV) to create complex fracture networks with high conductivity (Guo et al., 2023; Jiang et al., 2017; Wu et al., 2012). This reduces fluid flow distances in ultra-low permeability matrices from hundreds of meters to millimeters.

* Corresponding author.
** Corresponding author.
E-mail addresses: zangyuxi.syky@sinopec.com (Y.-X. Zang), tscsydx@163.com (S.-C. Tian).

Peer review under the responsibility of China University of Petroleum (Beijing).

Hydraulic fracturing, as the core SRV-enabling technology, has driven the North American shale revolution over the past decade. Nevertheless, conventional water-based fluids (e.g., slickwater, crosslinked gels) exhibit three inherent limitations (Lange et al., 2013; Tian et al., 2021; Vengosh et al., 2014; Wang et al., 2018; Zheng et al., 2022): (1) substantial water consumption, with single-well usage reaching 15,000–20,000 m^3, intensifying water-energy conflicts in arid regions such as the Permian Basin; (2) environmental risks from chemical-laden flowback fluids contaminating shallow aquifers, where treatment costs constitute 12%–18% of total development expenditures; and (3) formation damage due to aqueous phase trapping (APT), reducing near-fracture matrix permeability by 30%–70%, compounded by clay swelling that further constricts effective flow pathways. To overcome these constraints, waterless fracturing technologies have emerged as a frontier research focus (Li et al., 2021b; Wang et al., 2016; Zhang et al., 2019).

Among various waterless alternatives, CO_2 fracturing stands out due to its unique physicochemical properties: low interfacial tension (<5 mN/m), high diffusion coefficient (~10^{-7} m^2/s), organic matter dissolution capacity, and clay stabilization effect. Field evidence confirms its ability to enhance fracture complexity and estimated ultimate recovery (EUR) by 8%–15% (Esteves and Santos, 2019; Liu et al., 2014; Memon et al., 2022; Yang et al., 2017; Zang et al., 2023). However, the industrial implementation of pure CO_2 fracturing faces three critical engineering challenges that fundamentally limit its efficacy (Middleton et al., 2015; Pan et al., 2018; Zang et al., 2024): (1) high fluid loss due to low viscosity (0.02–0.08 cP), yielding leakoff coefficients 1–2 orders of magnitude higher than water-based fluids, which severely constrains fracture length; (2) poor proppant transport capacity, as proppant concentrations typically below 8% induce premature settling near wellbores, compromising far-field conductivity; and (3) phase sensitivity near the critical point (31.1 °C, 7.38 MPa), where minor pressure or temperature fluctuations trigger drastic density and viscosity variations, resulting in unstable fracture propagation.

It is precisely to overcome these inherent limitations of pure CO_2 fracturing that the CO_2 hybrid fracturing technique has been proposed as an innovative two-stage stimulation strategy (Carpenter, 2015; Lei et al., 2025; Li et al., 2021a; Zang et al., 2024). This methodology strategically harnesses the advantages of both fluids while mitigating their weaknesses. Stage I (Pre-injection of CO_2) leverages CO_2's high penetrability and geochemical reactivity to precondition the reservoir through rock weakening and generate initial fracture networks. Stage II (Conventional hydraulic fracturing) then utilizes the superior proppant-carrying capability of water-based fluids to extend fractures and ensure effective proppant placement, thereby directly addressing the core deficiencies of a pure CO_2 system.

The effectiveness of this hybrid approach is governed by the complex mechanisms of fracture initiation and propagation. In laminated shale formations, the presence of well-developed bedding planes introduces significant complexity to fracture behavior. Research has shown that CO_2-rock interaction can chemically weaken the rock fabric and bedding plane cementation through dissolution, thereby fundamentally altering the rock's mechanical response and subsequent fracture propagation trajectory (Esteves and Santos, 2019; Liu et al., 2014; Memon et al., 2022; Yang et al., 2017; Zang et al., 2023). However, a systematic, mechanistic understanding of how CO_2 pre-injection parameters quantitatively control fracture initiation pressure and resultant morphology remains an area of active investigation. This gap motivates the present study.

This study selects shale samples from the Chang-7 Member in the Ordos Basin as experimental specimens. Utilizing a self-developed hybrid CO_2 fracturing experimental apparatus, high-temperature and high-pressure hybrid CO_2 fracturing experiments simulating reservoir conditions were conducted. Based on CT scanning results, the fracture morphology under relevant engineering parameters—including fracturing fluid type, CO_2 exposure duration, and formation pore pressure—was quantitatively analyzed. This study reveals the influence mechanisms of CO_2 pre-injection on fracture propagation. The findings provide theoretical guidance for designing hybrid CO_2 fracturing process parameters in shale oil reservoirs.

2. Experimental methodology

2.1. Experimental device development

The hybrid CO_2 fracturing experiment employs a self-developed triaxial fracturing system comprising six key subsystems: a gas supply system (for CO_2 or N_2), a water supply system, a data control unit, a constant-temperature water bath, a triaxial core fracturing vessel, and a data acquisition system (Fig. 1). The integrated plunger pump within this system is capable of withstanding temperatures up to 80 °C and pressures up to

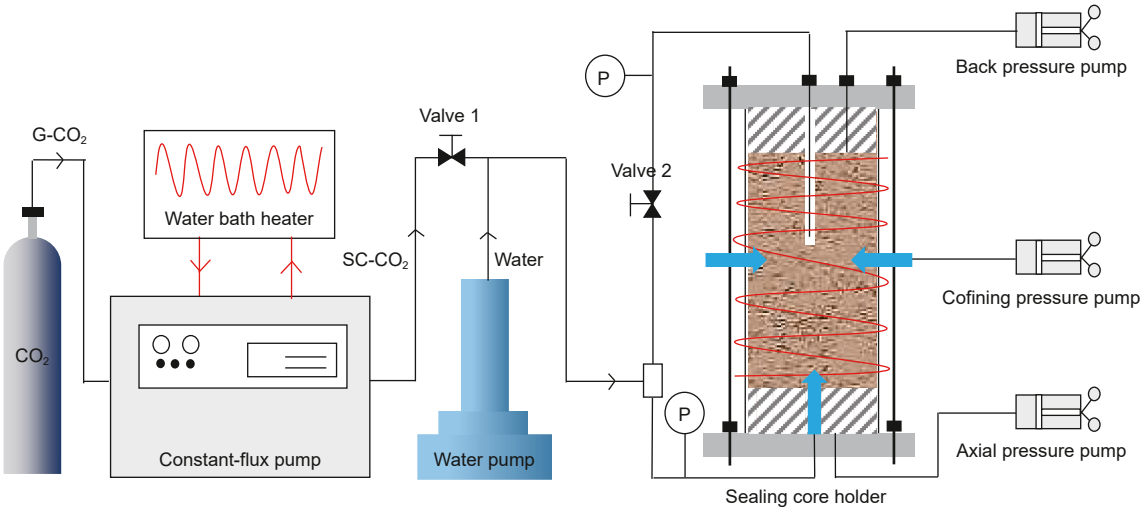

Fig. 1. Schematic diagram of hybrid CO_2 fracturing device (Zang et al., 2024).

80 MPa. Through coordinated operation with the water bath system, it achieves precise regulation of CO_2 temperature and pressure, enabling the transition of CO_2 into gaseous, liquid, or supercritical states. The data control unit manages the motor and vacuum pump, while the data acquisition system provides real-time monitoring of pressure and temperature variations, utilizing pressure sensors (0–50 MPa range, ±0.1 MPa accuracy) and temperature sensors (0–80 °C range, ±0.1 °C accuracy). Post-fracturing rock samples undergo non-destructive computed tomography (CT) scanning using a Zeiss 53 μm Micro-CT imaging system, facilitating quantitative analysis of characteristic fracture parameters including average fracture length, width, area ratio, and three-dimensional (3D) fractal dimension.

The triaxial core fracturing vessel, serving as the pivotal component of the CO_2 hybrid fracturing system, is designed to securely hold rock specimens and apply precisely controlled axial stress and confining pressure (hoop pressure). Fig. 2 illustrates the structural design of the improved triaxial core fracturing vessel employed in this study. This vessel is specifically engineered to accommodate standard cylindrical core specimens with a nominal diameter of 50 mm and a height of 100 mm. Adhering to stringent mechanical design tolerance specifications, the allowable maximum manufacturing deviation for the specimen diameter is ±0.05 mm, while the height is designed to be adjustable within a range of 95–105 mm, providing flexibility to meet diverse experimental requirements. A salient feature of this fracturing vessel is its compatibility with two distinct loading modes: rigid loading and flexible loading. When configured for rigid loading, the apparatus is capable of applying axial pressures of up to 100 MPa and confining pressures of up to 70 MPa, offering critical experimental capability for simulating rock mechanical behavior under complex geological conditions. To ensure absolute containment integrity and hermetic sealing throughout the high-pressure fluid environment of the experiment, both ends of the vessel are sealed with high-strength stainless steel end caps. Each end cap is meticulously fitted with one to two through-holes on its lateral surface. These holes function as essential access ports for the injection and discharge of fracturing fluid, facilitating the smooth execution of experimental procedures.

2.2. Experimental design and procedure

2.2.1. Specimen preparation

To ensure the comparability and reproducibility of fracturing results, all rock specimens were exclusively obtained from the Chang-7 shale formation in the Ordos Basin. Specifically, the samples were sourced from downhole cores of a designated well in the basin, at a depth of approximately 3500 m, where well-developed horizontal bedding is characterized. Prior to conducting fracturing experiments, a comprehensive suite of fundamental mechanical and physical property tests is performed on the specimens. These tests include uniaxial tensile strength tests, uniaxial compressive strength tests, porosity measurements, and permeability assessments (complete dataset available in Table 1). It is important to note that all mechanical property tests were conducted with the loading direction applied perpendicular to the bedding planes to ensure consistency and to characterize the properties most relevant to fracture propagation across the bedding. This establishes essential baseline properties for subsequent experimental analysis.

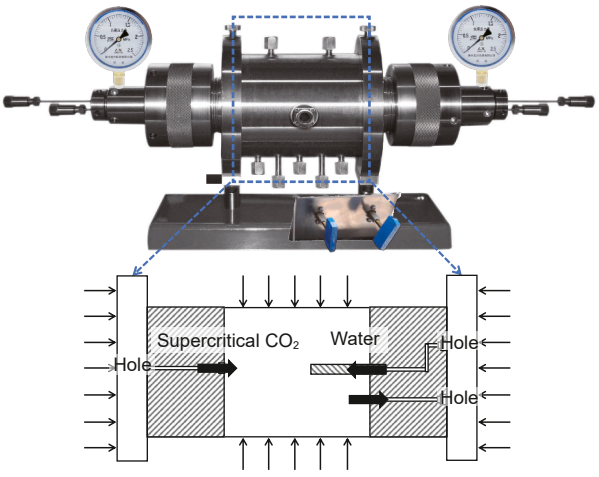

Fig. 2. Improved triaxial core fracturing vessel.

To accurately simulate hydraulic fracture propagation during horizontal well volumetric fracturing, irregular raw shale samples are precision-machined into standard cylindrical geometries (nominal dimensions: 50 mm diameter × 100 mm height) using a computer-numerically-controlled (CNC) wire saw cutting system, with cutting orientation perpendicular to the bedding planes. To authentically replicate downhole drilling conditions, a 9 mm diameter × 45 mm deep pilot borehole is drilled at the geometric center of each specimen. Custom-designed casing (8 mm outer diameter × 35 mm length) is precisely inserted into the borehole, and the annulus is permanently sealed with high-strength epoxy resin to simulate the well cementing process. Fracturing fluid is injected through the casing to apply pumping pressure within the 10 mm open-hole section, thereby replicating the core mechanism of hydraulic fracturing. Standard specimen dimensions and injection hole geometry parameters are detailed in Fig. 3.

2.2.2. Experimental procedure

The core focus of this study is to systematically investigate the influence of pre-pad fluid type, CO_2 exposure time, and formation pore pressure on the fracture propagation behavior of shale specimens under CO_2 hybrid fracturing conditions. Based on the geological characteristics of the target reservoir and field fracturing practices, this study strictly follows the orthogonal experimental design principles, formulating a comprehensive set of 11 experimental configurations, as detailed in Table 2. The design of the key experimental parameters relies on similarity theory and the similarity criteria derived from the Clifton fracture control equation, aiming to accurately simulate the actual fracturing environment of the target oilfield (Clifton and Abou-Sayed, 1979). During the derivation of the similarity criteria, significant consideration is given to actual fracturing conditions as well as the typical characteristics of shale reservoirs, such as the development of multiple fractures, low porosity, and low permeability. To effectively simulate the in-situ conditions of a shale reservoir at a depth of approximately 1500 m, while also ensuring the safety of the loading system, the confining pressure and axial pressure are set to 20 MPa and 25 MPa, respectively. According to the established similarity criteria, the in-situ stress and breakdown pressure are primarily controlled by the elastic modulus, while the injection rate and fracturing time are determined by the sample size. Additionally, the viscosity of the fracturing fluid is influenced by the sample dimensions, injection rate, and elastic modulus. Among the 11 experimental groups, experiments 1# to 5# are primarily designed to analyze the impact of pre-pad CO_2 injection time on fracture propagation patterns and effectiveness. Experiments 6# to 9# focus on examining the influence of formation pore pressure changes on fracture propagation, and experiments 10# and 11# are conducted to compare the fracturing effectiveness of a single-type fracturing fluid (i.e., without a pre-CO_2 injection

Table 1
Rock sample physical property test results.

No.	Permeability, 10^{-3} μm^2	Porosity, %	Uniaxial tensile strength, MPa	Uniaxial compressive strength, MPa	Young's modulus, GPa	Poisson's ratio
1	0.82	10.46	7.53	214.07	19.43	0.234
2	0.60	11.15	7.40	191.06	20.66	0.259
3	0.72	10.65	6.81	186.91	19.66	0.281
Average value	0.71	10.75	7.25	197.35	19.92	0.258

Note: All mechanical tests were conducted with loading direction perpendicular to bedding planes.

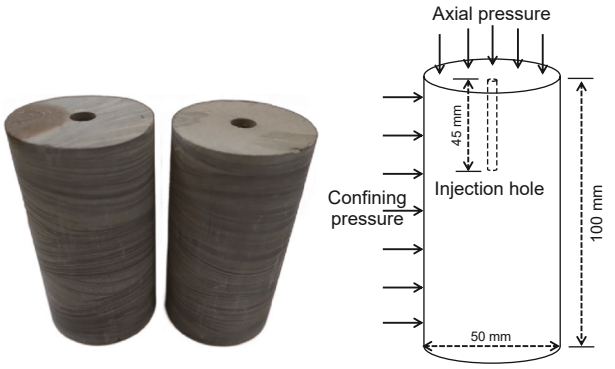

Fig. 3. Sample preparation and size information.

phase). It is important to note that the focus of this study is primarily on the impact mechanism of CO_2 pre-injection parameters (type and exposure time) on fracture propagation, and it does not consider the effects of subsequent water injection parameter changes. Therefore, a constant-pressure water injection method is employed during the experiments. Given that water has a much lower compressibility than gas, and to ensure operational safety and experimental comparability, the injection pressure of water is controlled to be lower than that of gas. Based on this principle, the water injection pressure is uniformly set to 15 MPa across all experiments.

Although each experimental condition was conducted once due to the complexity and cost of the triaxial fracturing tests, the high consistency in the physical and mechanical properties of the shale samples (Table 1) and the clear trends observed in breakdown pressure and fracture morphology across different groups support the reproducibility of the experimental outcomes. Future studies will include repeated tests under key conditions to further validate the results.

2.2.3. Experimental process

The detailed experimental procedure for hybrid CO_2 fracturing is as follows:

(1) Instrument installation

The cylindrical core specimen is secured within the triaxial fracturing cell, sealed, and connected to inlet/outlet pipelines, temperature sensors, pressure transducers, and monitoring systems.

(2) Specimen pretreatment

Selected core samples undergo degreasing and desalination washing, followed by oven-drying and mass recording. To ensure experimental accuracy, porosity, permeability, and mechanical properties are measured (detailed in Table 1). Vacuum-treated specimens are saturated by 48-h immersion in simulated formation water under 20 MPa confining pressure.

(3) Fracturing fluid phase control
1) Hydraulic fracturing stage: An ISCO high-pressure/high-precision syringe pump generates and injects fracturing fluid.
2) CO_2 fracturing stage: Phase-specific CO_2 is preconditioned and stored in an accumulator via a coordinated syringe pump-accumulator-thermostatic bath system.

Insulated short-path flow lines ensure negligible CO_2 parameter fluctuations, maintaining stable supercritical conditions.

(4) Stress field loading

The triaxial cell confines the specimen while manual hydraulic pumps apply axial pressure and confining pressure separately. Prior to pre-pad CO_2 injection, back pressure is applied using an independent hydraulic pump to ensure injection continuity and formation pressure stability.

(5) Staged fracturing implementation
1) Pre-pad CO_2 injection phase
Valve 1 opens and Valve 2 closes (Fig. 1) to achieve

Table 2
Experimental scheme.

Sample	Pre-pad fluid type	CO_2 exposure time, h	Injection pressure, MPa		Back pressure, MPa
			CO_2	water	
1#	CO_2	1	18	15	12
2#		2			
3#		4			
4#		6			
5#		8			
6#	CO_2	4	18	15	8
7#					10
8#					14
9#					16
10#	Water (only)	/	/	15	12
11#	CO_2 (only)	/	30	/	12

uniform injection through the specimen base. The lower right port (Fig. 2) serves as the CO_2 discharge outlet. Stable injection is confirmed when discharge pressure consistently matches and maintains ISCO injection pressure.

2) Aqueous fracturing fluid injection phase

Valve 1 closes and Valve 2 opens (Fig. 1). The ISCO pump injects aqueous fracturing fluid into the wellbore via the upper right port (Fig. 2). Hydraulic fracture propagation completion is identified by a sharp pressure drop at the injection port.

(6) Data analysis

Post-experiment, valves are closed and specimens cooled to ambient temperature before retrieval. Pumping pressure-time curves are integrated with 3D fracture morphology data from CT scanning to systematically analyze the influence mechanisms of fracturing fluid type, CO_2 exposure duration, and formation pore pressure on fracture propagation behavior.

2.3. Fracture quantitative evaluation index

Fracture dimensions and spatial complexity serve as critical metrics for evaluating fracturing efficacy. To systematically investigate the influence of engineering factors on fracture propagation behavior, a standardized quantitative assessment protocol established by our research group is implemented through three analytical criteria:

(1) Mean fracture length & width

Grayscale data from CT-scanned rock specimens undergo 3D reconstruction using PerGeos digital core analysis software (Fig. 4). An optimal global threshold for each sample was determined using the Otsu method to objectively differentiate the fracture voids from the rock matrix during binarization processing. Optimal threshold segmentation based on grayscale differentiation between rock matrix and fractures enables binarization processing. Digital algorithms then calculate mean fracture length and width from extracted fracture topology. Increases in these parameters directly indicate fracture dimension expansion, objectively reflecting enhanced fracturing performance.

(2) Fracture area ratio (AR)

Defined as the ratio of actual fracture surface area S_f to its orthogonally projected area S_p on the specimen base (excluding borehole area):

$$AR = \frac{S_f}{S_p} \tag{1}$$

where S_f denotes actual fracture area, mm^2, and S_p represents net projected area, mm^2. Rising AR values signify increased fracture network complexity and enlarged stimulated reservoir volume.

(3) 3D fractal dimension (FD)

This scalar metric quantifies geometrical complexity through power-law scaling. The FD was computed using the cube-counting algorithm (Zang et al., 2024). Let $N(\varepsilon)$ be the minimum number of spheres of radius ε required to cover the fractal structure:

$$N(\varepsilon) \propto \varepsilon^{-FD} \tag{2}$$

Higher FD values correlate with greater fracture surface irregularity and spatial complexity.

3. Experimental results and discussion

3.1. Effect of fracturing fluid type

As the core component of hydraulic fracturing technology, fracturing fluids perform critical functions in oilfield development, including pressure transmission and proppant transport. Selecting fluids optimized for shale reservoir characteristics significantly enhances stimulation efficiency. Under identical experimental conditions, this section compares the fracture propagation characteristics induced by different fluid systems. Specifically: Sample 10# underwent conventional hydraulic fracturing; Sample 11# utilized pure CO_2 fracturing; Sample 3# employed staged CO_2-water fracturing (pre-pad CO_2 followed by water). Detailed parameter configurations are provided in Table 2.

3.1.1. Pumping pressure-time curves

Pumping pressure-time curves during shale hydraulic fracturing exhibit consistent evolutionary patterns, systematically categorized into four sequential phases: initial pressurization phase, rapid pressurization phase, pressure decline phase, and pressure stabilization phase. Variations in fracturing conditions across core specimens manifest as significant differences in breakdown pressure magnitudes, time-to-fracture initiation, and curve morphological characteristics. Fig. 5(a) comparatively illustrates the dynamic pressure evolution profiles under three distinct fracturing fluid systems: water-based fluid, pure CO_2, and staged CO_2-water hybrid fluid (pre-pad CO_2 followed by water).

Analysis of the pumping pressure-time curve for Sample 10# (conventional hydraulic fracturing) reveals significantly shorter

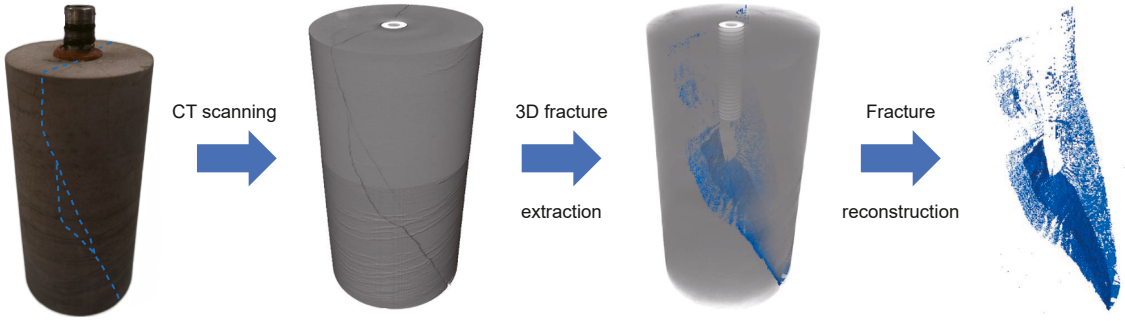

Fig. 4. Fracture quantification extraction and analysis process.

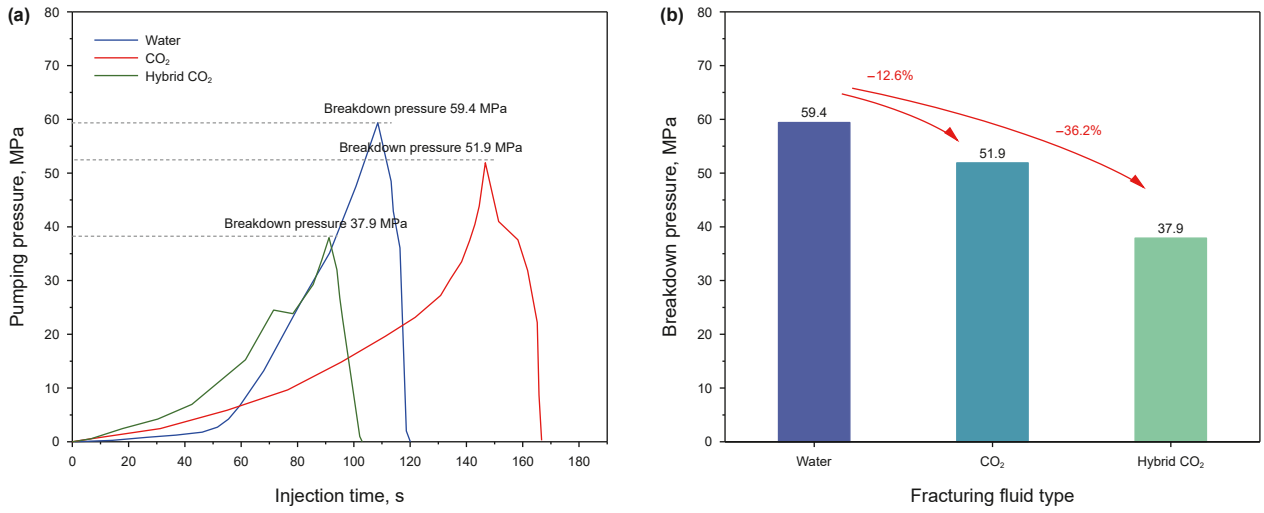

Fig. 5. Pumping pressure-time curve affected by fracturing fluid type. (**a**) Pumping pressure-time curves for different fracturing fluids; (**b**) breakdown pressure comparison.

pressurization duration compared to gaseous fluids, attributable to water's lower compressibility. Specifically, specimen failure occurred at 108.5 s with 59.4 MPa breakdown pressure, followed by an abrupt pressure decline indicating fracture initiation. Conversely, Sample 11# (CO_2 fracturing) exhibited gradual pressure escalation due to CO_2's higher compressibility, reduced interfacial tension, lower viscosity, and enhanced micro-pore penetrability. Fracture initiation commenced at 146.7 s (51.9 MPa breakdown pressure), with subsequent pressure stabilization rather than immediate decline—a phenomenon resulting from sustained rock-breaking capacity during supercritical CO_2 phase transition into miscible fluids, before gradual pressure decay. For Sample 3# (pre-pad CO_2-water hybrid fracturing), the pressure rise rate was markedly slower than conventional fracturing. A precursor pressure drops at 71.5 s signaled localized fracture initiation, preceding specimen-wide fracture propagation at 91.2 s with 37.9 MPa breakdown pressure. These observations conclusively demonstrate the pronounced influence of fracturing fluid rheology on pressure-time profiles.

Experimental data in Fig. 5(b) demonstrate that Sample 10# (conventional hydraulic fracturing) exhibits the highest breakdown pressure of 59.4 MPa. Comparatively, Sample 11# (pure CO_2 fracturing) shows a 12.6% reduction in breakdown pressure (51.9 MPa). Most significantly, Sample 3# (pre-pad CO_2 injection followed by water fracturing) achieves a breakdown pressure of 37.9 MPa, representing a 36.2% decrease relative to conventional fracturing. These findings establish that: Conventional fracturing requires the highest breakdown pressure; pure CO_2 fracturing moderately reduces breakdown pressure; pre-pad CO_2 hybrid fracturing substantially lowers breakdown pressure. This systematic pressure reduction hierarchy conclusively demonstrates the technical advantages of CO_2 hybrid fracturing stimulation protocols.

3.1.2. Fracture expansion morphology

Comparative analysis of fracture propagation morphology under different fracturing fluids was conducted using X-ray micro-computed tomography (in μCT), with reconstructed 3D fracture networks presented in Fig. 6 (blue regions denote hydraulic fractures, HF). Sample 10# (conventional hydraulic fracturing) exhibits a relatively simple longitudinal fracture (Fig. 6(a)) initiating from the base of the open-hole section. This fracture propagates vertically along the maximum principal stress direction (perpendicular to bedding planes), displaying linear geometry with minimal surface tortuosity. The core specimen remains structurally intact without secondary fracture generation. For Sample 11# (pure CO_2 fracturing), Fig. 6(b) reveals fracture initiation at the lower open-hole section - attributed to CO_2's high penetrability requiring extended pressure diffusion to reach breakdown threshold. While propagating along the σHmax direction, the fracture demonstrates pronounced curvature and surface roughness. This non-throughgoing fracture preserves core integrity without complete specimen failure. Sample 3# (pre-pad CO_2-water hybrid fracturing) develops complex fracture networks (Fig. 6(c)). The primary HF initiates at the open-hole section and extends along σHmax. Crucially, CO_2 preconditioning weakens rock mechanical properties (28% tensile strength reduction), enabling: Two bedding-parallel branch fractures bifurcating from the main HF; A horizontal secondary fracture along basal bedding planes. This multi-planar system demonstrates significantly enhanced complexity compared to mono-fluid treatments.

Quantitative characterization of post-fracture morphology via μCT and PerGeos digital analysis (Fig. 7) reveals that staged CO_2-water fracturing enhances fractal dimension by 8.3% and 7.3% compared to conventional and pure CO_2 methods respectively. Pre-pad CO_2 injection increases fracture length by 4.9% over conventional fracturing, while pure CO_2 extends length by 5.1%—though this improvement remains modest relative to hybrid stimulation. The fixed injection volume induces a width-length tradeoff: pre-pad CO_2 reduces aperture by 13.3% versus conventional methods but generates 2.57 × wider fractures than pure CO_2. Crucially, pre-pad CO_2 achieves peak fracture area ratio values (1.52 × conventional; 2.58 × pure CO_2), demonstrating simultaneous enhancement of fracture dimensions (length: +4.9%, width: +157% vs pure CO_2) and network complexity (FD: +8.3%). These metrics establish CO_2 hybrid fracturing as a technically superior strategy for comprehensive reservoir stimulation.

Based on the aforementioned research on rock breakdown pressure and fracture propagation morphology, it is substantiated that pre-pad CO_2 injection into shale reservoirs dissolves in formation brine to form dilute carbonic acid solution. This reactive fluid chemically interacts with calcite, dolomite, orthoclase, and anorthite in shale through the following geochemical reactions (Romanov et al., 2015):

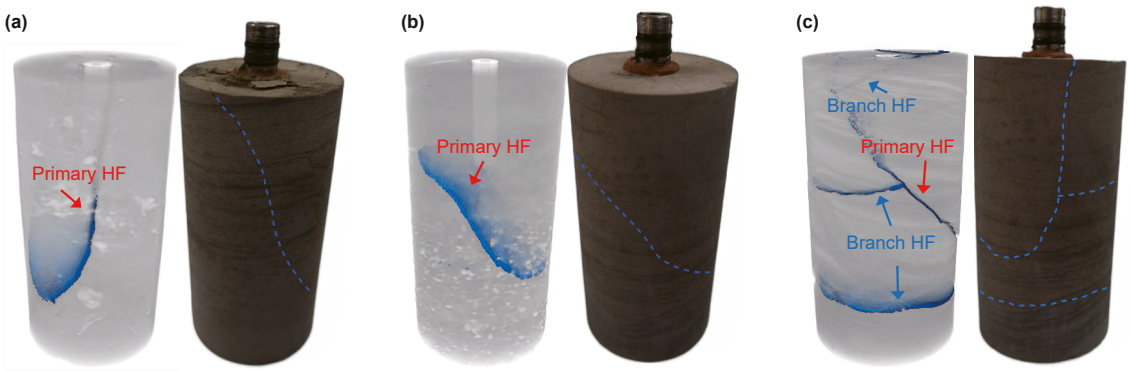

Fig. 6. Fracture propagation morphology affected by fracturing fluid type. (**a**) Water; (**b**) CO_2; (**c**) hybrid CO_2.

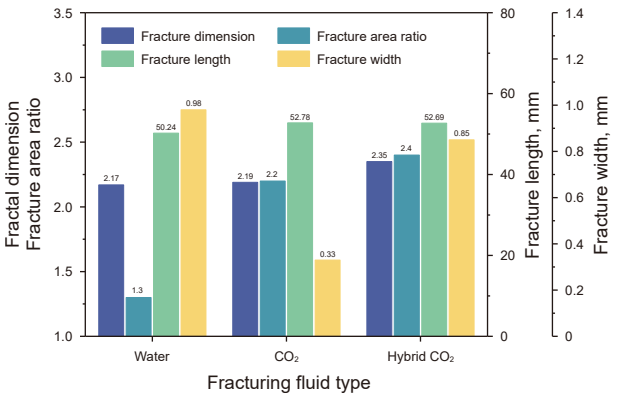

Fig. 7. Quantitative evaluation of fractures under the influence of fracturing fluid type.

$$\text{Calcite} + 2H^+ \leftrightarrow Ca^{2+} + CO_2 + H_2O \quad (3)$$

$$\text{Dolomite} + 4H^+ \leftrightarrow Ca^{2+} + Mg^{2+} + 2CO_2 + 2H_2O \quad (4)$$

$$\text{Orthoclase} + 2H^+ + H_2O \leftrightarrow 2K^+ + Al_2Si_2O_5(OH)_4 + 4SiO_2 \quad (5)$$

$$\text{Anorthite} + 2H^+ + H_2O \leftrightarrow Ca^{2+} + Al_2Si_2O_5(OH)_4 \quad (6)$$

Chemical reactions between CO_2 and shale reservoir minerals not only alter mineral composition and pore architecture but also induce significant rock strength degradation. As substantiated in Figs. 8 and 9, this manifests as marked reductions in uniaxial compressive strength (UCS) and elastic modulus of treated specimens. Consequently, pre-pad CO_2 injection facilitates: Reduced breakdown pressure during hydraulic fracturing; enhanced fracture complexity. These mechanochemical effects collectively underscore the technical superiority of CO_2 hybrid fracturing. Therefore, subsequent investigations in this research program will primarily focus on optimizing this hybrid stimulation methodology.

3.2. Effect of CO_2 exposure time

During the pre-pad CO_2 injection phase, fluid-rock interactions fundamentally alter shale's physical and mechanical properties, thereby governing reservoir stimulation efficacy. The CO_2 exposure duration serves as a critical determinant of fracturing outcomes, as established in prior research (Romanov et al., 2015). Under controlled experimental conditions, this section comparatively analyzes the influence of pre-pad CO_2 exposure time on fracture propagation characteristics. Field operational data from literature and industry practice indicate that pre-pad CO_2 injection typically spans 0.5–3 days in actual reservoir treatments. Through dimensional analysis scaling reservoir drainage volume to laboratory core dimensions, this corresponds to 1–8 h of core-scale exposure time. Accordingly, we designate five experimental durations: 1, 2, 4, 6, and 8 h. Complete parameter specifications are provided in Table 2.

3.2.1. Pumping pressure-time curves

Initial CO_2 exposure time exerts significant influence on fracture initiation and propagation processes. Under identical experimental conditions, Fig. 10 illustrates corresponding pressure-time curves for aqueous fracturing fluid injection across varying pre-pad CO_2 exposure durations. All curves consistently exhibit four sequential stages: initial pressurization, rapid pressure buildup, pressure decline, and pressure stabilization.

The pumping pressure-time curves exhibit distinct evolutionary patterns under varying pre-pad CO_2 exposure durations. For short exposure times (1–2 h), the pressure response resembles conventional hydraulic fracturing (Sample 10#), with Sample 1# (1 h) fracturing abruptly at 101.6 s (56.2 MPa breakdown pressure). As exposure time increases (2–8 h), CO_2-induced rock degradation reduces the initial pressurization phase duration (Fig. 10, red zone) and accelerates failure, shortening breakdown times to 97.4 s (2 h), 91.2 s (4 h), 86.3 s (6 h), and 72.8 s (8 h). Specifically, for rock Sample 4# subjected to CO_2 for 6 h, at an injection time of 67.6 s, the pumping pressure reached 14.3 MPa followed by a slight drop, indicating the formation of localized small-scale fractures at this point. After 6 h, the rate of decrease in breakdown pressure significantly diminished, suggesting a stabilizing trend in the weakening effect. Similarly, Sample 5# exposed to CO_2 for 8 h exhibited a comparable trend. However, due to the longer CO_2 exposure time, the rock experienced more pronounced mechanical degradation, leading to two minor breakdowns occurring at 49.7 s and 61.9 s. These trends demonstrate that extended CO_2 exposure (1) reduces pressurization time by 28.4%, (2) decreases time-to-failure by 28.4%, and (3) increases precursor fracture activity (pressure fluctuations +28.7%), collectively enhancing fracture initiation efficiency through chemical-mechanical rock weakening.

Comparative analysis of breakdown pressures in CO_2 pre-pad fracturing (Fig. 10(f)) demonstrates significant exposure time dependency. Relative to conventional hydraulic fracturing (59.4 MPa), extended CO_2 exposure progressively reduces breakdown pressure: 56.2 MPa (−5.4%) at 1 h, 52.3 MPa (−12.0%) at 2 h,

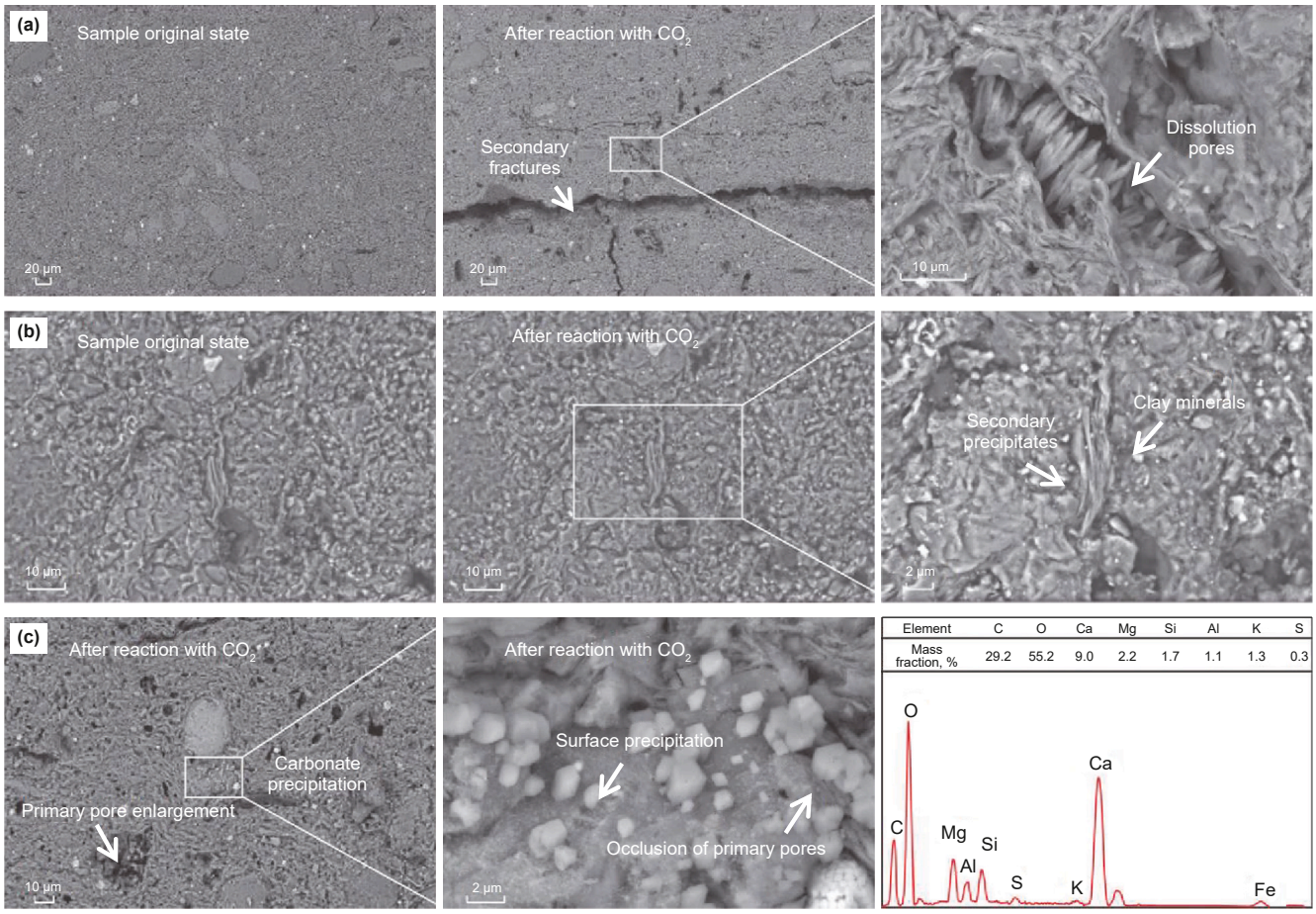

Fig. 8. Based on micro-morphological characterization of shale minerals before and after CO_2 reaction (adapted from reference (Dai et al., 2023)). (**a**) Calcite dissolution features; (**b**) clay mineral alteration; (**c**) carbonate rock with precipitated mineral EDS spectra (Future investigations employing in-situ characterization techniques would be highly valuable to provide a direct, time-resolved visualization of the geochemical processes).

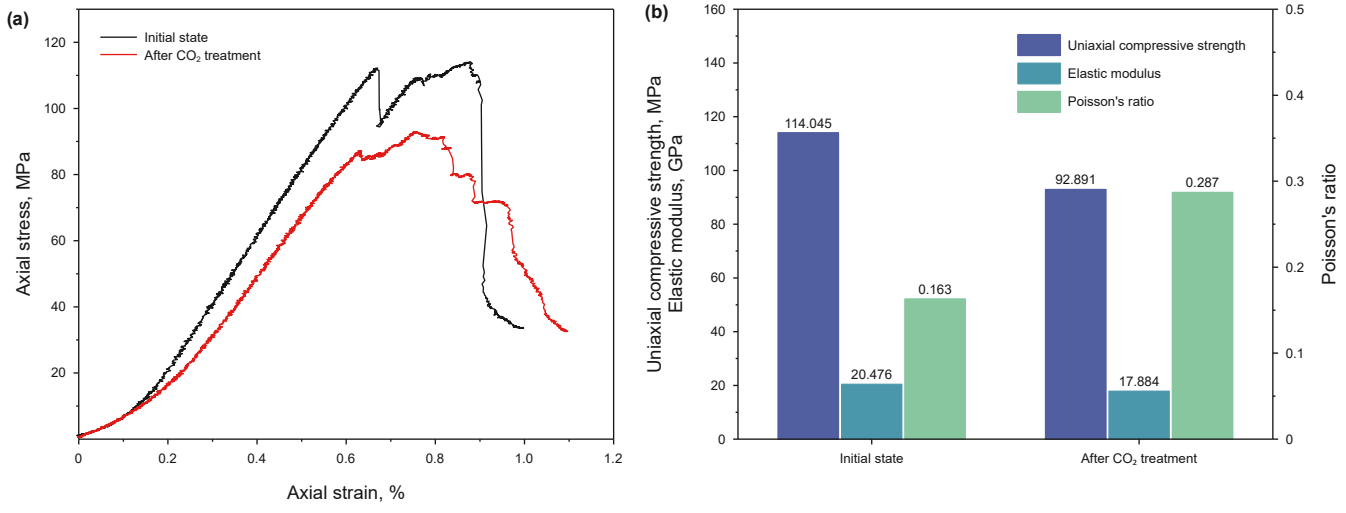

Fig. 9. Changes in rock mechanical properties before and after CO_2 reaction (Adapted from reference (Sun et al., 2023)). (**a**) Stress-strain curve; (**b**) fundamental mechanical properties.

37.9 MPa (−36.2%) at 4 h, 33.1 MPa (−44.3%) at 6 h, and 31.2 MPa (−47.5%) at 8 h. Compared to the 1-h baseline, prolonged exposure achieves additional reductions of 6.9% (2 h), 32.6% (4 h), 41.1% (6 h), and 44.5% (8 h). These trends establish that: (1) Short-term exposure (≤1 h) yields limited pressure reduction (<6%) and marginal stimulation efficacy. (2) The inverse pressure-time correlation exhibits asymptotic saturation beyond 6 h, where incremental gains diminish substantially (only 3.2% reduction from

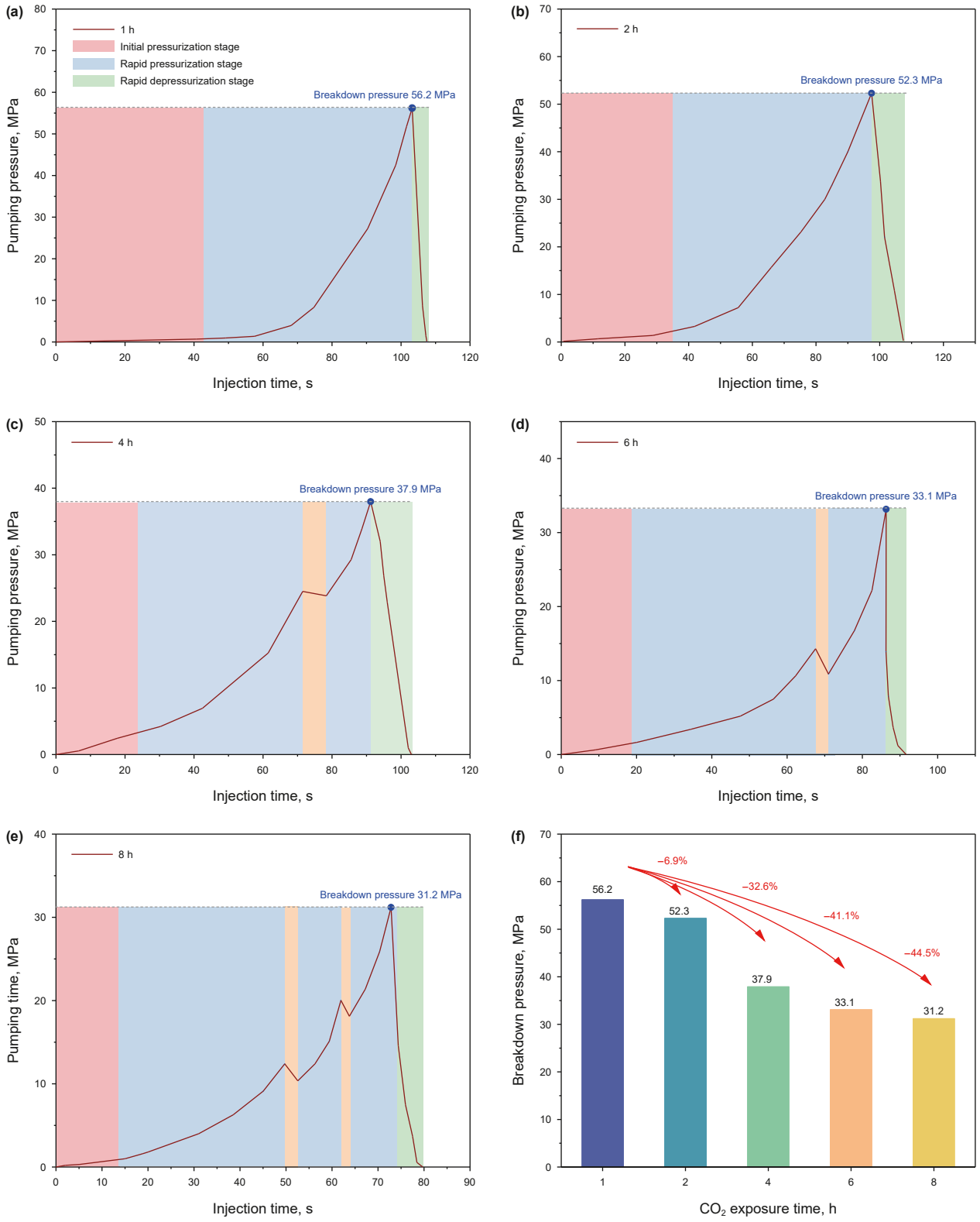

Fig. 10. Pump pressure-time curve under the influence of CO_2 exposure time. (**a**) Pumping pressure-time curves for CO_2 exposure times of 1 h; (**b**) pumping pressure-time curves for CO_2 exposure times of 2 h; (**c**) pumping pressure-time curves for CO_2 exposure times of 4 h; (**d**) pumping pressure-time curves for CO_2 exposure times of 6 h; (**e**) pumping pressure-time curves for CO_2 exposure times of 8 h; (**f**) breakdown pressure vs. exposure time.

6 h → 8 h versus 30.8% from 1 h → 6 h), indicating stabilized rock degradation beyond this threshold. This observation aligns with previous studies, confirming that the most significant geochemical reactions and mechanical weakening occur during the initial hours of CO_2-shale interaction, after which the reaction rate slows considerably (Dilshan and Perera, 2024; Gao et al., 2024).

3.2.2. Fracture expansion morphology

Comparative CT analysis reveals that CO_2 exposure time significantly influences fracture propagation morphology (Fig. 11). For Sample 1# (1-h pre-pad CO_2), hydraulic fracturing generates a longitudinal fracture initiating from the open-hole section, propagating along the maximum principal stress direction with regular geometry and smooth surface (Fig. 11(a)). Compared to conventional fracturing, this fracture extends to the specimen base and penetrates the bottom surface, causing complete failure. In Sample 2# (2-h exposure), localized rock degradation triggers secondary fracture initiation when the primary fracture extends into weakened zones, forming bedding-parallel secondary fractures (Fig. 11(b)). For Sample 5# (8-h exposure), the main fracture connects two rock weakness planes during propagation along σHmax, developing branched fractures; rock fragments detach during specimen retrieval, with significantly increased fracture surface roughness (Fig. 11(d)).

Quantitative analysis of post-fracture morphology (Fig. 12) demonstrates that prolonged CO_2 exposure time significantly enhances fracture dimensions and complexity. Relative to the 1-h baseline, extending exposure to 2, 4, and 8 h increases mean fracture width by 19.4%, 37.1%, and 43.5% respectively, while fracture length rises by 2.6%, 2.7%, and 3.8%. Fractal dimension—quantifying complexity—increases by 1.8%, 6.3%, and 7.7%, with the most pronounced enhancement observed in fracture area ratio (+13.3%, +60.0%, +73.3%). These nonlinear progressions indicate intensified morphological development under extended exposure, establishing 4 h as the optimal threshold for synergistic dimension-complexity optimization under experimental conditions.

Pre-pad CO_2 injection induces alterations in rock mechanical strength and physical properties, critically influencing proppant embedment and placement during subsequent slurry injection. This study demonstrates that exposure duration significantly governs fracturing effectiveness through integrated analysis of breakdown pressure and fracture morphology. As established in Section 3.1.2, prolonged CO_2-rock interaction triggers geochemical reactions that generate mechanically weakened planes, substantially reducing rock strength. This degradation facilitates complex fracture network development during hydraulic fracturing by lowering initiation resistance. However, when the CO_2 exposure duration is excessively prolonged, the geochemical reactions tend to stabilize, resulting in a diminished impact on reservoir properties. Future work will involve detailed mineralogical analysis to precisely quantify the temporal evolution of rock degradation. Consequently, excessive extension provides marginal efficacy improvement while incurring unnecessary CO_2 resource expenditure. Field implementation therefore requires precise optimization of pre-pad injection duration to maximize stimulation benefits.

3.3. Effect of formation pore pressure

Formation pore pressure—defined as the fluid pressure within subsurface rock pores and fractures (Wang et al., 2020b)—elevates continuously during sustained pre-pad CO_2 injection. Owing to the low permeability of rock matrices, this process generates a high-pressure zone near the wellbore that significantly governs the orientation and dimensions of subsequently generated hydraulic fractures (Fig. 13). Herein, we define effective pore pressure as the differential between CO_2 injection pressure and backpressure. Under identical experimental conditions, systematic investigation of fracture propagation characteristics was conducted across varying pore pressures (10, 8, 6, 4, 2 MPa), with detailed parameters provided in Table 2.

3.3.1. Pumping pressure-time curves

Pumping pressure profiles during aqueous fracturing fluid injection exhibit significant variations under different formation pore pressures. At 10 MPa pore pressure (Fig. 14(a)), Sample 6# displays multiple pressure peaks at 24.1, 31.9, 41.5, and 69.3 s, with ultimate failure occurring at 78.4 s. Reducing pore pressure to 8 MPa (Sample 7#, Fig. 14(b)) yields a single pressure drop at 37.2 s preceding complete failure at 83.0 s. At 4 MPa (Sample 8#, Fig. 14(d)), extended initial nonlinear pressurization culminates in rapid pressure decline at 101.5 s, indicating major fracture generation. Further reduction to 2 MPa (Sample 9#, Fig. 14(e)) produces pressure-time behavior resembling conventional hydraulic fracturing, with fracture initiation at 104.9 s, demonstrating negligible pre-pad CO_2 influence under ultralow pore pressure conditions.

Comparative analysis of breakdown pressures across varying formation pore pressures (Fig. 14(f)) reveals an inverse correlation: decreasing pore pressure elevates breakdown pressure systematically. At 10 MPa pore pressure, breakdown pressure measures 30.5 MPa. Reduction to 8 MPa increases it to 34.6 MPa (+13.4%). Further decrease to 6 MPa yields 37.9 MPa (+24.3% vs 10 MPa). At 4 MPa, breakdown pressure rises to 46.5 MPa, culminating at 54.9 MPa under 2 MPa conditions—merely 7.6% below conventional hydraulic fracturing (59.4 MPa). These measurements demonstrate that elevated pore pressure reduces effective stress

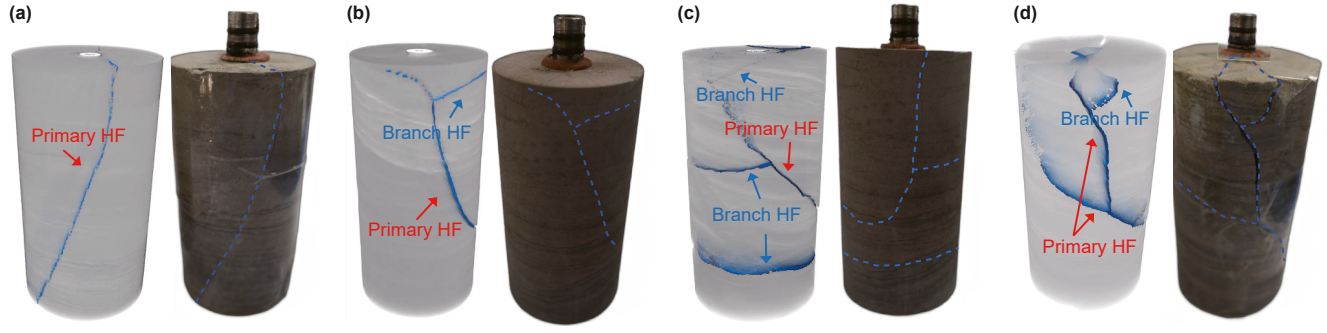

Fig. 11. Fracture propagation morphology under the influence of CO_2 exposure time. (**a**) 1 h; (**b**) 2 h; (**c**) 4 h; (**d**) 8 h.

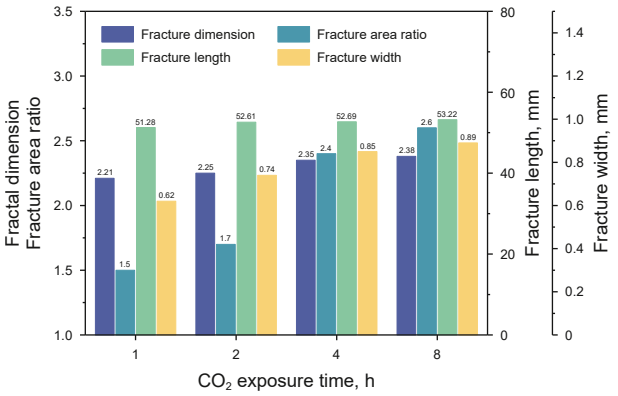

Fig. 12. Quantitative evaluation of fractures under the influence of CO_2 exposure time.

on rock matrices, facilitating fracture initiation. However, marginal pore pressure increases (e.g., <4 MPa differential) yield diminishing stimulation returns.

3.3.2. Fracture expansion morphology

CT-based analysis of fracture morphology under varying pore pressures (Fig. 15) reveals significant pressure-dependent characteristics. At 10 MPa (Sample 6#), substantial energy supplementation from pre-pad CO_2 drastically reduces effective stress on shale matrices. Combined with mechanically weak, highly compressible bedding planes, this condition promotes "fishbone-like" branched fractures where the main fracture connects upper bedding layers, resulting in severe specimen fragmentation upon retrieval – demonstrating exceptional stimulation efficacy. At 8 MPa (Sample 7#), CO_2-induced pressure elevation preferentially opens bedding planes, generating multiple bedding-parallel fractures that form complex interconnected networks with ideal stimulation outcomes. Conversely, at 2 MPa (Sample 9#), fracture propagation resembles conventional water fracturing: a primary fracture initiates from the open-hole section, extends perpendicular to bedding along σHmax, and develops a single bedding-parallel branch at mid-lower weak interfaces. This limited complexity confirms marginal stimulation efficacy under ultralow pore pressure conditions.

Quantitative evaluation of post-fracture characteristics under varying pore pressures (Fig. 16) demonstrates that elevated pore pressure enhances fracture length during CO_2-preconditioned fracturing. When pore pressure increases to 2, 4, 6, 8, and 10 MPa via pre-pad CO_2 injection, fracture length rises from the conventional fracturing baseline (50.24 m) to 50.36 m (+0.2%), 52.69 m (+4.9%), 54.78 m (+9.0%), and 57.32 m (+14.1%) respectively. Given constant injected fluid volume, this length extension inversely reduces fracture width to 0.92 m (−6.1%), 0.85 m (−13.3%), 0.72 m (−26.5%), and 0.51 m (−47.9%) at corresponding pressures. Complexity metrics show consistent increases: fractal dimension rises by 0.9%, 8.3%, 15.7%, and 21.7%, while fracture area ratio exhibits more pronounced gains of 23.1%, 84.6%, 107.7%, and 123.1%. These trends confirm that pore pressure elevation significantly improves fracture length and complexity at the cost of width reduction—substantially impairing fracture conductivity. Notably, marginal pressure increases (≤2 MPa) yield negligible stimulation enhancement.

The reduction in fracture width under elevated pore pressure can be attributed to the decrease in effective normal stress acting on the fracture faces. According to the effective stress principle, the normal effective stress σ_n' is given by:

$$\sigma_n' = \sigma_n - \alpha P_p \tag{7}$$

where σ_n is the total normal stress, P_p is the pore pressure, and α is the Biot coefficient. As P_p increases, σ_n' decreases, reducing the normal closure stress on the fracture. This promotes fracture initiation and extension along bedding planes but limits the aperture opening due to the reduced compressive confinement. Consequently, while fracture length and complexity increase, the width is constrained, leading to a trade-off between fracture dimensions and conductivity.

Integrated findings demonstrate that enhanced formation energy intensifies shale matrix compaction, increasing grain packing density while reducing porosity. This process elevates Poisson's ratio, decreases elastic modulus and compressive strength, and reduces effective stress (Lin et al., 2025), collectively destabilizing the reservoir and ultimately triggering structural failure. Pre-pad CO_2 injection replenishes formation energy, locally amplifying pressure and stress fields to facilitate fracture propagation and reorientation during hydraulic fracturing, thereby enhancing network complexity. Concurrently, CO_2 activates closed natural microfractures and bedding planes near the wellbore, synergistically improving subsequent stimulation efficacy. Crucially, excessive pore pressure elevation in field operations yields marginal fracturing improvement but risks exceeding downhole equipment pressure ratings. Therefore, design protocols must integrate geological constraints and equipment safety thresholds to ensure operational feasibility and onsite safety.

3.4. Discussion

The laboratory-scale findings presented in this study, while obtained under controlled and scaled conditions, provide crucial mechanistic insights that align with and help explain observations from field-scale CO_2 fracturing operations in shale reservoirs, such as those conducted in the Ordos Basin.

A consistent trend reported from field applications is the notable reduction in treating pressure during hybrid CO_2-water fracturing compared to conventional hydraulic fracturing (Dai et al., 2026; Lei et al., 2025). This directly corroborates our laboratory measurement of a 36.2% decrease in breakdown pressure for the hybrid method (Sample 3#) compared to hydraulic fracturing (Sample 10#). The underlying mechanism—geochemical weakening of the rock matrix and the elevation of pore pressure

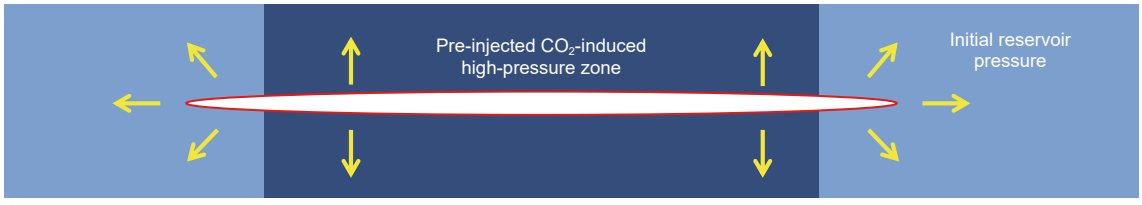

Fig. 13. Formation pressure affects fracture propagation.

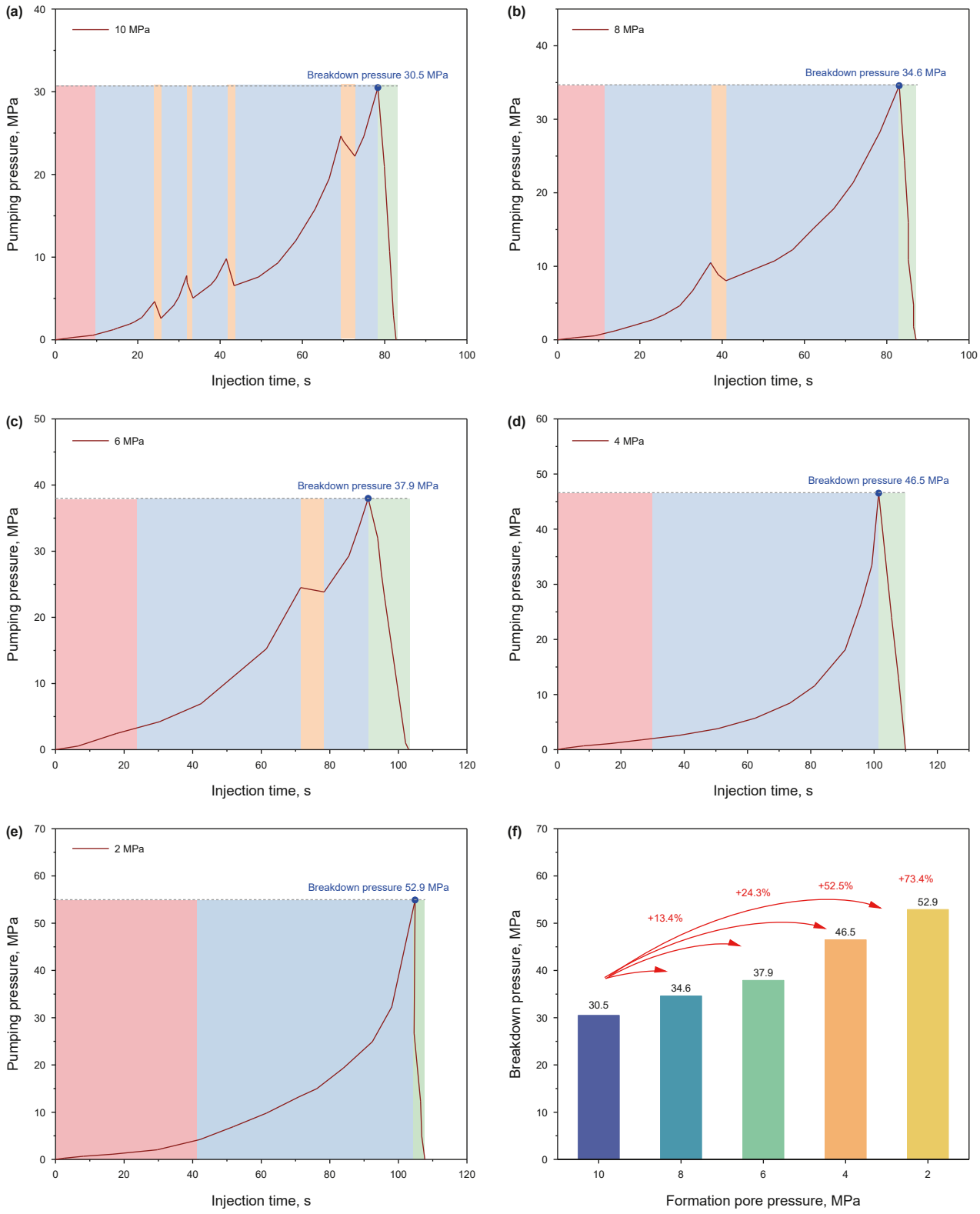

Fig. 14. Pump pressure-time curve under the influence of formation pore pressure. (**a**) Pumping pressure-time curves under 10 MPa pore pressures; (**b**) pumping pressure-time curves under 8 MPa pore pressures; (**c**) pumping pressure-time curves under 6 MPa pore pressures; (**d**) pumping pressure-time curves under 4 MPa pore pressures; (**e**) pumping pressure-time curves under 2 MPa pore pressure; (**f**) breakdown pressure vs. pore pressure.

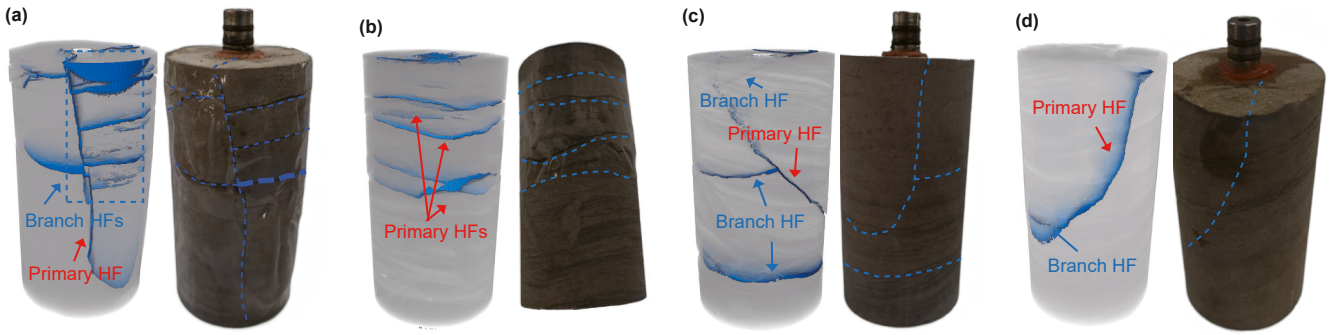

Fig. 15. Fracture propagation patterns under the influence of formation pore pressure. (**a**) 10 MPa; (**b**) 8 MPa; (**c**) 6 MPa; (**d**) 2 MPa.

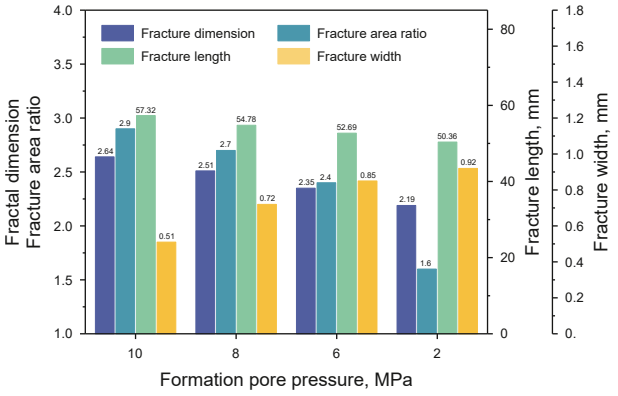

Fig. 16. Quantitative evaluation of fractures under the influence of formation pore pressure.

due to pre-pad CO_2 injection—is universal across scales. In the field, this translates to lower pump requirements and potential cost savings. Furthermore, the enhanced complexity of the fracture network generated by the hybrid method, quantitatively demonstrated by the significant increases in Fracture Area Ratio and Fractal Dimension in our experiments (Section 3.1.2), is a primary objective in field-scale "volume fracturing". Field diagnostics, such as microseismic monitoring, often indicate more diffuse and complex event clouds during CO_2-involved stimulations, suggesting better activation of natural fractures and bedding planes, which is consistent with the complex, multi-branched fracture morphologies observed in our CT scans (e.g., Figs. 6(c) and 11(c)–(d)).

Beyond the immediate fracturing efficacy, the findings of this study highlight the dual-significance of CO_2 hybrid fracturing in enhancing hydrocarbon recovery and contributing to carbon sequestration. The significant extension of fracture length (up to 14.1%) and the dramatic increase in fracture network complexity (Fractal Dimension increased by up to 21.7%) directly imply a larger contact area between the fracture system and the reservoir matrix. This is a critical factor for enhancing the recovery factor in ultra-low permeability shale reservoirs. A more complex and extensive fracture network can lead to a higher estimated ultimate recovery (EUR), with field pilots often reporting EUR enhancements of 8%–15% for CO_2-based fracturing compared to conventional methods. Concurrently, the process entails the injection and containment of a substantial volume of CO_2 within the formation. While the primary mechanism is physical trapping in the created fracture network and adjacent pores, the geochemical interactions described in Section 3.1.2 can lead to mineral trapping over longer timescales, further stabilizing the stored CO_2. Although a precise quantitative assessment of storage capacity requires reservoir-scale modeling, the laboratory-verified mechanisms of rock weakening and complex fracture creation provide a positive indicator for the technical feasibility of combining enhanced oil recovery (CO_2-EOR) with carbon storage utilization (CSU) in shale oil reservoirs.

It is, however, critical to acknowledge the scaling challenges. While the trends and mechanisms are consistent, direct quantitative extrapolation of laboratory values (e.g., absolute fracture length in millimeters) to field dimensions (fracture length in tens of meters) is not appropriate. Differences arise due to factors such as the greater complexity and heterogeneity of in-situ stress fields over hundreds of meters, continuous fluid leak-off into a vast natural fracture network, and the dynamic propagation over much longer timescales in the field. Our experimental design, utilizing similarity criteria, aimed to capture the dominant physics rather than replicate the absolute field scale.

In conclusion, the excellent alignment between the fundamental mechanisms revealed in this laboratory study and the empirical observations from the field strongly enhances the credibility of our findings. Our work provides a scientific foundation for interpreting field data and optimizing operational parameters, such as pre-pad CO_2 soaking time and injection strategy, to maximize the effectiveness of hybrid CO_2 fracturing in shale reservoirs like the Chang-7 member.

While the laboratory-scale experiments provide valuable insights into the mechanisms of CO_2 hybrid fracturing, several factors must be considered when scaling up to field applications. These include:

(1) In-situ stress heterogeneity: Field-scale stress variations may lead to more complex fracture propagation paths.
(2) Fluid loss and leak-off: The high diffusivity of CO_2 may result in significant fluid loss in natural fracture systems, affecting fracture length and network complexity.
(3) Fracture height confinement: In layered reservoirs, stress barriers may restrict vertical fracture growth.
(4) CO_2 phase behavior: Temperature and pressure gradients in the reservoir can cause phase changes, influencing fracture initiation and propagation.

Future work should incorporate large-scale simulations and field trials to validate and adapt these laboratory findings to real-world conditions.

4. Conclusions

This investigation conducted hybrid CO_2 fracturing experiments under simulated reservoir conditions for the Chang-7 shale formation, Ordos Basin, utilizing a self-developed experimental system. By controlling key engineering parameters—including fracturing fluid type, CO_2 exposure duration, and formation pore pressure—coupled with quantitative CT characterization, the study elucidates fracture propagation mechanisms and geometric response characteristics, yielding the following key findings:

(1) Fracturing fluid type: CO_2 hybrid fracturing demonstrates distinct advantages over both conventional hydraulic fracturing and pure CO_2 fracturing. It significantly reduces the breakdown pressure by 36.2% compared to hydraulic fracturing. Furthermore, it not only increases fracture dimensions but also substantially enhances fracture network complexity, evidenced by an 8.3% and 7.3% increase in fractal dimension, and a 1.52-times and 2.58-times increase in fracture area ratio, respectively.

(2) CO_2 exposure time: The pre-pad CO_2 exposure time is a critical parameter governing fracturing efficacy. As the exposure time increases, the rock breakdown pressure shows a pronounced decreasing trend, with a maximum reduction of 47.5% observed after 8 h. Concurrently, both fracture dimensions and structural complexity exhibit marked increases, with the most significant enhancement occurring within the first 4–6 h.

(3) Formation pore pressure: Increasing formation pore pressure during pre-pad CO_2 injection promotes the activation of mechanically weak bedding planes. This leads to significant enhancements in fracture length (up to 14.1%) and complexity (fractal dimension increased by 21.7%). However, this process simultaneously restricts the widening of fracture apertures, reducing fracture width by 47.9% and potentially impairing fracture conductivity.

(4) Underlying mechanism: The synergy in CO_2 hybrid fracturing stems from a sequential mechanism. Pre-injected CO_2 pre-conditiones the shale reservoir by inducing geochemical reactions that weaken the rock matrix and elevate pore pressure. The subsequent hydraulic fracturing then efficiently propagates fractures through this pre-weakened zone, resulting in lower initiation pressure and a more complex fracture network.

CRediT authorship contribution statement

Yu-Xi Zang: Writing – review & editing, Writing – original draft, Software, Methodology, Investigation, Data curation, Conceptualization. **Feng-Xia Li:** Writing – review & editing. **Hai-Zhu Wang:** Writing – review & editing, Methodology, Conceptualization. **Zhi-Wen Huang:** Supervision. **Tong Zhou:** Writing – review & editing. **Jia Cui:** Writing – review & editing. **Ning Li:** Writing – review & editing. **Shou-Ceng Tian:** Supervision, Conceptualization.

Declaration of competing interest

The authors declare that they have no known competing financial interests or personal relationships that could have appeared to influence the work reported in this paper.

Acknowledgments

The work was supported by the National Science and Technology Major Project on New Types of Oil and Gas Exploration and Development “Innovative Technologies in Oil and Gas Field Geomechanics and Reservoir Stimulation” (2025ZD1401400) and “Advanced Waterless Stimulation Technology for High-Stress Reservoirs” (2025ZD1401406).

References

Avanthi Isaka, B.L., Ranjith, P.G., Rathnaweera, T.D., 2019. The use of super-critical carbon dioxide as the working fluid in enhanced geothermal systems (EGSs): A review study. Sustain. Energy Technol. Assessments 36, 100547. https://doi.org/10.1016/j.seta.2019.100547.

Carpenter, C., 2015. Use of a CO_2-hybrid fracturing design to enhance production. J. Petrol. Technol. 67, 118–120. https://doi.org/10.2118/0715-0118-JPT.

Clifton, R.J., Abou-Sayed, A.S., 1979. On the computation of the three-dimensional geometry of hydraulic fractures. In: Symposium on Low Permeability Gas Reservoirs. https://doi.org/10.2118/7943-MS.

Dai, X., Wang, M., Feng, G., et al., 2023. Mineralogical erosion and precipitation characteristics and their effects on adsorption property of shale during $scCO_2$-H_2O-shale interaction. J. China Coal Soc. 48 (7), 2813–2826. https://doi.org/10.13225/j.cnki.jccs.CN23.3265.

Dai, X., Wei, J., Li, Y., et al., 2026. Study on parameters influencing fracture propagation and the influence of sensitive parameters on CO_2 enhanced oil reservoirs in Gulong shale oil. Geoenergy Sci. Eng. 257, 214197. https://doi.org/10.1016/j.geoen.2025.214197.

Dilshan, R.A.D.P., Perera, M.S.A., 2024. Effect of mechanical weakening and crack formation on caprock integrity during underground hydrogen storage in depleted gas reservoirs – A comprehensive review. Fuel 371, 131893. https://doi.org/10.1016/j.fuel.2024.131893.

Esteves, A.F., Santos, F.M., 2019. Carbon dioxide as geothermal working fluid: An overview. Renew. Sustain. Energy Rev. 114, 109331. https://doi.org/10.1016/j.rser.2019.109331.

Gao, B., Li, Y., Pang, Z., et al., 2024. Geochemical mechanisms of water/CO_2-rock interactions in EGS and its impacts on reservoir properties: A review. Geothermics 118, 102923. https://doi.org/10.1016/j.geothermics.2024.102923.

Guo, J., Lu, Q., Liu, Z., et al., 2023. Concept and key technology of “multi-scale high-density” fracturing technology: A case study of tight sandstone gas reservoirs in the western Sichuan Basin. Nat. Gas. Ind. B 10 (3), 283–292. https://doi.org/10.1016/j.ngib.2023.05.005.

Jiang, T., Bian, X., Wang, H., et al., 2017. Volume fracturing of deep shale gas horizontal wells. Nat. Gas. Ind. B 4 (2), 127–133. https://doi.org/10.1016/j.ngib.2017.07.018.

Lange, T., Sauter, M., Heitfeld, M., Schetelig, et al., 2013. Hydraulic fracturing in unconventional gas reservoirs: Risks in the geological system part 1. Environ. Earth Sci. 70 (8), 3839–3853. https://doi.org/10.1007/s12665-013-2803-3.

Lei, Z., Meng, S., Peng, Y., et al., 2025. Evaluation of the adaptability of CO_2 prefracturing to Gulong shale oil reservoirs, Songliao Basin, NE China. Petrol. Explor. Dev. 52 (2), 459–470. https://doi.org/10.1016/S1876-3804(25)60579-9.

Li, L., Chen, Z., Su, Y.L., et al., 2021. Experimental investigation on enhanced-oil-recovery mechanisms of using supercritical carbon dioxide as prefracturing energized fluid in tight oil reservoir. SPE J. 26 (5), 3300–3315. https://doi.org/10.2118/202279-PA%JSPEJournal.

Li, N., Wang, C., Zhang, S., et al., 2021. Recent advances in waterless fracturing technology for the petroleum industry: An overview. J. Nat. Gas Sci. Eng. 92, 103999. https://doi.org/10.1016/j.jngse.2021.103999.

Lin, S., Chang, X., Yang, C., et al., 2025. Integrated supercritical CO_2 injection for shale reservoir enhancement: Mechanisms, experimental insights, and implications for energy and carbon storage. Energy 324, 135908. https://doi.org/10.1016/j.energy.2025.135908.

Liu, H., Wang, F., Zhang, J., et al., 2014. Fracturing with carbon dioxide: application status and development trend. Petrol. Explor. Dev. 41 (4), 513–519. https://doi.org/10.1016/S1876-3804(14)60060-4.

Lopez, G., Pourjamal, Y., Breyer, C., 2025. Paving the way towards a sustainable future or lagging behind? An ex-post analysis of the international energy agency's world energy outlook. Renew. Sustain. Energy Rev. 212, 115371. https://doi.org/10.1016/j.rser.2025.115371.

Memon, S., Feng, R., Ali, M., Bhatti, et al., 2022. Supercritical CO_2-Shale interaction induced natural fracture closure: implications for $scCO_2$ hydraulic fracturing in shales. Fuel 313, 122682. https://doi.org/10.1016/j.fuel.2021.122682.

Middleton, R.S., Carey, J.W., Currier, R.P., et al., 2015. Shale gas and non-aqueous fracturing fluids: opportunities and challenges for supercritical CO_2. Appl. Energy 147, 500–509. https://doi.org/10.1016/j.apenergy.2015.03.023.

Pan, Y., Hui, D., Luo, P., et al., 2018. Experimental investigation of the geochemical interactions between supercritical CO_2 and shale: Implications for CO_2 storage in gas-bearing shale formations. Energy Fuel. 32 (2), 1963–1978. https://doi.org/10.1021/acs.energyfuels.7b03074.

Romanov, V., Soong, Y., Carney, C., et al., 2015. Mineralization of carbon dioxide: A literature review. ChemBioEng Rev. 2, 231–256. https://doi.org/10.1002/cben.201500002.

Sun, L., Wang, H., Wang, B., et al., 2023. The effect of $SCCO_2$ treatments on the petrophysical properties of continental shale with different mineral compositions. In: 57th U.S. Rock Mechanics/Geomechanics Symposium. https://doi.org/10.56952/ARMA-2023-0467.

Tian, F., Liu, X., Zhang, S., et al., 2021. Continuous sand fracturing technology with slick water for continental shale oil in the dagang oilfield. Petrol. Drill. Tech. 49 (4), 118–124. https://doi.org/10.11911/syztjs.2021021.

Vengosh, A., Jackson, R.B., Warner, N., et al., 2014. A critical review of the risks to water resources from unconventional shale gas development and hydraulic fracturing in the United States. Environ. Sci. Technol. 48 (15), 8334–8348. https://doi.org/10.1021/es405118y.

Wang, F., Wang, L., 2022. Pore structure analysis and permeability prediction of shale oil reservoirs with HPMI and NMR: A case study of the Permian lucaogou formation in the Jimsar Sag, Junggar Basin, NW China. J. Petrol. Sci. Eng. 214, 110503. https://doi.org/10.1016/j.petrol.2022.110503.

Wang, H., Li, G., He, Z., et al., 2018. Experimental investigation on abrasive supercritical CO_2 jet perforation. J. CO2 Util. 28, 59–65. https://doi.org/10.1016/j.jcou.2018.09.018.

Wang, J., Wu, S., Li, Q., et al., 2020. Characterization of the pore-throat size of tight oil reservoirs and its control on reservoir physical properties: A case study of the Triassic tight sandstone of the sediment gravity flow in the Ordos Basin, China. J. Petrol. Sci. Eng. 186, 106701. https://doi.org/10.1016/j.petrol.2019.106701.

Wang, L., Yao, B., Cha, M., et al., 2016. Waterless fracturing technologies for unconventional reservoirs-opportunities for liquid nitrogen. J. Nat. Gas Sci. Eng. 35, 160–174. https://doi.org/10.1016/j.jngse.2016.08.052.

Wang, Y., Li, H., Qiao, L., et al., 2020. Reasonable degree of formation pressure maintenance in low permeability reservoirs. Chem. Technol. Fuels Oils 56 (3), 492–503. https://doi.org/10.1007/s10553-020-01160-4.

Wu, Q., Xu, Y., Wang, X., et al., 2012. Volume fracturing technology of unconventional reservoirs: connotation, design optimization and implementation. Petrol. Explor. Dev. 39 (3), 377–384. https://doi.org/10.1016/S1876-3804(12)60054-8.

Yang, F., Xie, C., Xu, S., et al., 2017. Supercritical methane sorption on organic-rich shales over a wide temperature range. Energy Fuel. 31 (12), 13427–13438. https://doi.org/10.1021/acs.energyfuels.7b02628.

Yu, H., Xu, H., Fan, J., et al., 2020. Transport of shale gas in microporous/nanoporous media: Molecular to pore-scale simulations. Energy Fuel. 35 (2), 911–943. https://doi.org/10.1021/acs.energyfuels.0c03276.

Zang, Y.X., Wang, H.Z., Wang, B., et al., 2024. In-situ laboratory study on influencing factors of pre-SC-CO_2 hybrid fracturing effect in shale oil reservoirs. Pet. Sci. 21 (5), 3547–3557. https://doi.org/10.1016/j.petsci.2024.05.020.

Zang, Y., Wang, Q., Wang, H., et al., 2023. Laboratory visualization of supercritical CO_2 fracturing in tight sandstone using digital image correlation method. Geoenergy Sci. Eng. 225, 211556. https://doi.org/10.1016/j.geoen.2023.211556.

Zhang, Z., Mao, J., Yang, X., et al., 2019. Advances in waterless fracturing technologies for unconventional reservoirs. Energy sources, part A: Recovery, utilization. Environ. Eff. 41 (2), 237–251. https://doi.org/10.1016/j.jngse.2016.08.052.

Zheng, Y., Wang, H., Tian, G., et al., 2022. Experimental investigation of proppant transport in hydraulically fractured wells using supercritical CO_2. J. Petrol. Sci. Eng. 217, 110907. https://doi.org/10.1016/j.petrol.2022.110907.

Zou, C., Lin, M., Ma, F., et al., 2024. Development, challenges and strategies of natural gas industry under carbon neutral target in China. Petrol. Explor. Dev. 51 (2), 476–497. https://doi.org/10.1016/S1876-3804(24)60038-8.